

Article

Predictive Modeling and Control Strategies for the Transmission of Middle East Respiratory Syndrome Coronavirus

Bibi Fatima ¹, Mehmet Yavuz ^{2,*} , Mati ur Rahman ³ , Ali Althobaiti ⁴  and Saad Althobaiti ⁵

¹ Department of Mathematics, University of Malakand, Chakadara 18800, Pakistan; fatma.uom@gmail.com

² Department of Mathematics and Computer Sciences, Faculty of Science, Necmettin Erbakan University, 42090 Konya, Türkiye

³ Department of Computer Science and Mathematics, Lebanese American University, Beirut 11022801, Lebanon; matimaths374@gmail.com

⁴ Department of Mathematics, College of Science, Taif University, P.O. Box 11099, Taif 21944, Saudi Arabia; aa.althobaiti@tu.edu.sa

⁵ Department of Sciences and Technology, Ranyah University Collage, Taif University, P.O. Box 11099, Taif 21944, Saudi Arabia; snthobaiti@tu.edu.sa

* Correspondence: mehmetyavuz@erbakan.edu.tr

Abstract: The Middle East respiratory syndrome coronavirus (MERS-CoV) is a highly infectious respiratory illness that poses a significant threat to public health. Understanding the transmission dynamics of MERS-CoV is crucial for effective control and prevention strategies. In this study, we develop a precise mathematical model to capture the transmission dynamics of MERS-CoV. We incorporate some novel parameters related to birth and mortality rates, which are essential factors influencing the spread of the virus. We obtain epidemiological data from reliable sources to estimate the model parameters. We compute its basic reproduction number (R_0). Stability theory is employed to analyze the local and global properties of the model, providing insights into the system's equilibrium states and their stability. Sensitivity analysis is conducted to identify the most critical parameter affecting the transmission dynamics. Our findings revealed important insights into the transmission dynamics of MERS-CoV. The stability analysis demonstrated the existence of stable equilibrium points, indicating the long-term behavior of the epidemic. Through the evaluation of optimal control strategies, we identify effective intervention measures to mitigate the spread of MERS-CoV. Our simulations demonstrate the impact of time-dependent control variables, such as supportive care and treatment, in reducing the number of infected individuals and controlling the epidemic. The model can serve as a valuable tool for public health authorities in designing effective control and prevention strategies, ultimately reducing the burden of MERS-CoV on global health.

Keywords: MERS-CoV model; basic reproductive number; analysis of stability; equilibria points; optimality control; numerical analysis



Citation: Fatima, B.; Yavuz, M.; ur Rahman, M.; Althobaiti, A.; Althobaiti, S. Predictive Modeling and Control Strategies for the Transmission of Middle East Respiratory Syndrome Coronavirus. *Math. Comput. Appl.* **2023**, *28*, 98. <https://doi.org/10.3390/mca28050098>

Academic Editor: Cristiana João Soares da Silva

Received: 26 May 2023

Revised: 8 September 2023

Accepted: 26 September 2023

Published: 30 September 2023



Copyright: © 2023 by the authors. Licensee MDPI, Basel, Switzerland. This article is an open access article distributed under the terms and conditions of the Creative Commons Attribution (CC BY) license (<https://creativecommons.org/licenses/by/4.0/>).

1. Introduction

The first identification of the Middle East respiratory syndrome coronavirus (MERS-CoV), a viral respiratory illness, took place in Saudi Arabia in 2012, as reported by multiple studies, including those conducted by [1–3]. MERS-CoV is believed to have originated from an animal source and has been identified in both humans and animals. The transmission of the disease occurs through close contact with an infected individual, in any form. The World Health Organization (2019) has reported a global total of 2519 laboratory-confirmed cases of MERS-CoV infection, with 866 associated deaths. One of the largest outbreaks of MERS-CoV occurred in South Korea in 2015.

Coronaviruses constitute a diverse family of viruses that are known to infect humans, causing respiratory illnesses that can vary in severity from mild cold-like symptoms to severe respiratory syndromes, such as severe acute respiratory syndrome (SARS). MERS-CoV

can cause zoonotic infections in humans through direct or indirect contact with camels or camel-related products. Additionally, human-to-human transmission has been reported, particularly in healthcare settings [4–6]. Since 2002, three novel coronaviruses have emerged and caused deadly zoonotic diseases in humans. The first was SARS, which emerged in November 2002. The second was MERS, which emerged in April 2012. The most recent and ongoing pandemic is COVID-19, which emerged in December 2019 and has affected millions of people worldwide [7–10]. The authors in [11,12] modified a mathematical model of COVID-19 by including the quarantine class and measured the disease transmission. Shen et al. studied a mathematical model of COVID-19 by presenting the vaccinated class with an optimal control analysis [13]. The authors in [14] used the data of Saudi Arabia and investigated the transmission dynamics of COVID-19. Tsay et al. analyzed the state estimation and optimal control for the COVID-19 outbreak model in the US [15]. Libotte et al. used the optimal strategy for vaccines in COVID-19 treatment considered for both mono- and multi-objective optimization [16]. Using the optimal control models also gives information about the impact of individual vaccination during an epidemic, together with the key considerations for political and economic decision making.

MERS typically presents with symptoms such as fever, cough, and shortness of breath. It is believed to spread through respiratory secretions, such as through coughing, from an infected person, similar to other coronaviruses. Several studies have investigated the potential role of camel handlers in the transmission of the virus to determine its source of infection. To understand and predict the dynamics of infectious diseases, researchers have developed various models based on biologically feasible parameters [17–19]. These models are essential tools for analyzing and forecasting the spread of diseases [20]. Although several case studies have explored the transmission of MERS-CoV, the literature on its transmission dynamics is limited. Using available data, Cauchemez et al. [21] estimated the incubation period and generation time of MERS-CoV, and calculated the reproductive numbers for both animal-to-human and human-to-human transmission. Chowell et al. [22] took a different approach and compared the reproductive numbers of SARS and MERS. Assiri et al. [23] reported one of the largest outbreaks of MERS-CoV, describing the virus as transmissible from human to human. The virus has spread globally through travel-associated cases, with reported incidences in countries including Algeria, Austria, China, Egypt, Italy, Netherlands, Philippines, South Korea, Thailand, the UK, and the US. Ground-breaking research has been published by numerous esteemed researchers, delving into the exploration of various model types, such as: SIR epidemic models [24,25], the discrete-time prey–predator model [26], and the memristor system [27]. Several infectious disease models have been investigated by researchers by using different approaches, which are available in the literature, such as [28–32].

Members of the coronavirus family, MERS-CoV and COVID-19 (caused by SARS-CoV-2) have certain similarities. It is crucial to remember that these viruses are diverse from one another and have distinctive traits and effects on human health. The following examples demonstrate how MERS-CoV can be used to treat various illnesses, including COVID-19. Both COVID-19 and MERS-CoV can cause serious respiratory infections in people. However, their overall effects differ considerably in a number of ways. MERS-CoV and COVID-19 can also be compared to influenza viruses, particularly those that cause severe respiratory infections. Different influenza viruses (A, B, and C) are what cause the illness. Despite the fact that some symptoms and the means of transmission are similar, influenza viruses have unique genetic traits and often create seasonal outbreaks. However, MERS-CoV and SARS-CoV-2 can cause pandemics or sporadic epidemics with ongoing human-to-human transmission. Several researchers have suggested mathematical models by applying different approaches to an infectious disease and studying its dynamics from different angles [33–37].

As far as the novelty is concerned, we study the model presented in [38], by incorporating the natural birth rate and death rate due to MERS-CoV. We modified the mathematical model for MERS-CoV transmission dynamics. This model consists of six

groups: susceptible class \mathcal{S} , exposed class (or high risk latent) \mathcal{E} , symptomatic and infectious class \mathcal{I} , infectious but asymptomatic class \mathcal{A} , hospitalized class \mathcal{H} , and recovery class \mathcal{R} . After constructing the model, the basic reproductive number is calculated by using the next generation method, and the local and global stability of the equilibrium points are determined. Lyapunov function theory is then utilized to analyze the global behavior of the model. Furthermore, the principles of optimal control theory are employed to reduce the number of infected persons and maximize the recovery rate within a given population.

2. Model Formulation

Here, we study the mathematical formulation of the deterministic model for MERS-CoV, using a set of differential equations. Specifically, the model describes the dynamics of the host population using the following system of equations:

$$\begin{aligned}
 \dot{\mathcal{S}}(t) &= bN - \frac{\varphi \mathcal{I} \mathcal{S}}{N} - \frac{\varphi q \mathcal{H} \mathcal{S}}{N} - \eta_0 \mathcal{S}, \\
 \dot{\mathcal{E}}(t) &= \frac{\varphi \mathcal{I} \mathcal{S}}{N} + \frac{\varphi q \mathcal{H} \mathcal{S}}{N} - (\chi + \eta_0) \mathcal{E}, \\
 \dot{\mathcal{I}}(t) &= \chi \xi \mathcal{E} - (\vartheta_a + \vartheta_1) \mathcal{I} - (\eta_0 + \eta_1) \mathcal{I}, \\
 \dot{\mathcal{A}}(t) &= \chi(1 - \xi) \mathcal{E} - (\eta_0 + \eta_2) \mathcal{A}, \\
 \dot{\mathcal{H}}(t) &= \vartheta_a \mathcal{I} - \vartheta_\theta \mathcal{H} - \eta_0 \mathcal{H}, \\
 \dot{\mathcal{R}}(t) &= \vartheta_1 \mathcal{I} + \vartheta_\theta \mathcal{H} - \eta_0 \mathcal{R},
 \end{aligned} \tag{1}$$

with initial conditions

$$\mathcal{S}(0) \geq 0, \mathcal{E}(0) \geq 0, \mathcal{I}(0) \geq 0, \mathcal{A}(0) \geq 0, \mathcal{H}(0) \geq 0, \mathcal{R} \geq 0,$$

where the used parameters in the above system are: bN represents the rate of birth for the host populace, while the transmission rate from human to human per unit time is represented by φ . The parameter q determines the relative transmissibility of hospitalized individuals. χ represents the rate at which individuals transition from the exposed compartment \mathcal{E} to the infectious compartment \mathcal{I} . The proportion of individuals who progress from \mathcal{E} to \mathcal{I} is given by ξ , while the remaining $(1 - \xi)$ progress to class \mathcal{A} . The average rate at which symptomatic persons are hospitalized is denoted by ϑ_a , while ϑ_1 represents the rate of recovery without hospitalization, and ϑ_θ represents the rate of recovery of hospitalized patients. The rate of natural death is represented by η_0 , while η_1 and η_2 represent deaths due to MERS-CoV.

Assume that the total populace is represented by $N(t)$ at time t , and satisfies $N(t) = \mathcal{S} + \mathcal{E} + \mathcal{I} + \mathcal{A} + \mathcal{H} + \mathcal{R}$.

Adding all the equations of system (1), we have

$$\frac{dN}{dt} = bN - \eta_0 \mathcal{S} - \eta_0 \mathcal{E} - (\eta_0 + \eta_1) \mathcal{I} - (\eta_0 + \eta_2) \mathcal{A} - \eta_0 \mathcal{H} - \eta_0 \mathcal{R}.$$

Therefore, from the above relation for biological applications, the considered system (1) occurred in the closed set as

$$\mathbb{F} = \left\{ (\mathcal{S}, \mathcal{E}, \mathcal{I}, \mathcal{A}, \mathcal{H}, \mathcal{R}) \in \mathcal{R}_+^6, 0 < \mathcal{S} + \mathcal{E} + \mathcal{I} + \mathcal{A} + \mathcal{H} + \mathcal{R} \leq \frac{bN}{\eta_0} \right\}.$$

3. Basic Reproduction Number

The basic reproduction number determines whether an epidemic will appear or the infection will die out. It represents the expected average number of new infections that will be generated by a single infective person, both directly and indirectly, when introduced into a fully susceptible populace. In this study, we use the approach of Driessche and

Watmough [39,40] to calculate the basic reproduction number for the aforementioned system (1).

$$F = \begin{bmatrix} 0 & \frac{\varphi S_0}{N} & \frac{\varphi q S_0}{N} \\ 0 & 0 & 0 \\ 0 & 0 & 0 \end{bmatrix}, V = \begin{bmatrix} \chi + \eta_0 & 0 & 0 \\ -\chi \zeta & (\vartheta_a + \vartheta_1) + (\eta_0 + \eta_1) & 0 \\ 0 & -\vartheta_a & \vartheta_\vartheta + \eta_0 \end{bmatrix} \tag{2}$$

to find

$$FV^{-1} = \begin{pmatrix} \frac{\chi \varphi \zeta S_0 (\vartheta_\vartheta + \eta_0 + q \vartheta_a) \mathcal{I}}{N(\chi + \eta_0)(\vartheta_\vartheta + \eta_0)[(\vartheta_a + \vartheta_1) + (\eta_0 + \eta_1)]} & \frac{\varphi S_0 (\vartheta_\vartheta + \eta_0 + q \vartheta_a)}{N(\vartheta_\vartheta + \eta_0)[(\vartheta_a + \vartheta_1) + (\eta_0 + \eta_1)]} & \frac{\varphi S_0 q}{N[(\vartheta_\vartheta + \eta_0)(\vartheta_a + \vartheta_1) + (\eta_0 + \eta_1)]} \\ 0 & 0 & 0 \\ 0 & 0 & 0 \end{pmatrix}.$$

Thus, the required basic reproduction number R_0 is followed by

$$R_0 = \frac{\chi \varphi \zeta S_0 Q_1}{N(\chi + \eta_0) Q_2 Q_3}.$$

The terms Q_1 , Q_2 , and Q_3 are defined as follows:

$$Q_1 = (\vartheta_\vartheta + \eta_0 + q \vartheta_a);$$

$$Q_2 = (\vartheta_\vartheta + \eta_0);$$

$$Q_3 = (\vartheta_a + \vartheta_1) + (\eta_0 + \eta_1).$$

These terms correspond to the susceptible individuals at the disease-free equilibrium (DFE).

Analysis of Sensitivity

Here, we conduct a sensitivity analysis of some of the parameters used in the model. This technique helps us to identify the parameters that have a significant effect on the basic reproduction number (See Table 1 and Figure 1). We use the approach as described by Chintis [41] to calculate the sensitivity index of R_0 . Specifically, the sensitivity index $\Delta_h^{R_0}$ of a parameter h is presented by the formula $\Delta_h^{R_0} = \frac{\partial R_0}{\partial h} \frac{h}{R_0}$.

Table 1. Sensitivity indices of different parameters.

Notation	Sensitivity Values	Notation	Sensitivity Values
χ	0.0384651	ϑ_1	− 0.058565
ϑ_ϑ	−0.00000453	ϑ_a	−0.93704
η_0	−0.001464128	η_1	−0.041392
φ	0.99999	q	0.0000476
bN	0.99999	ζ	0.000432

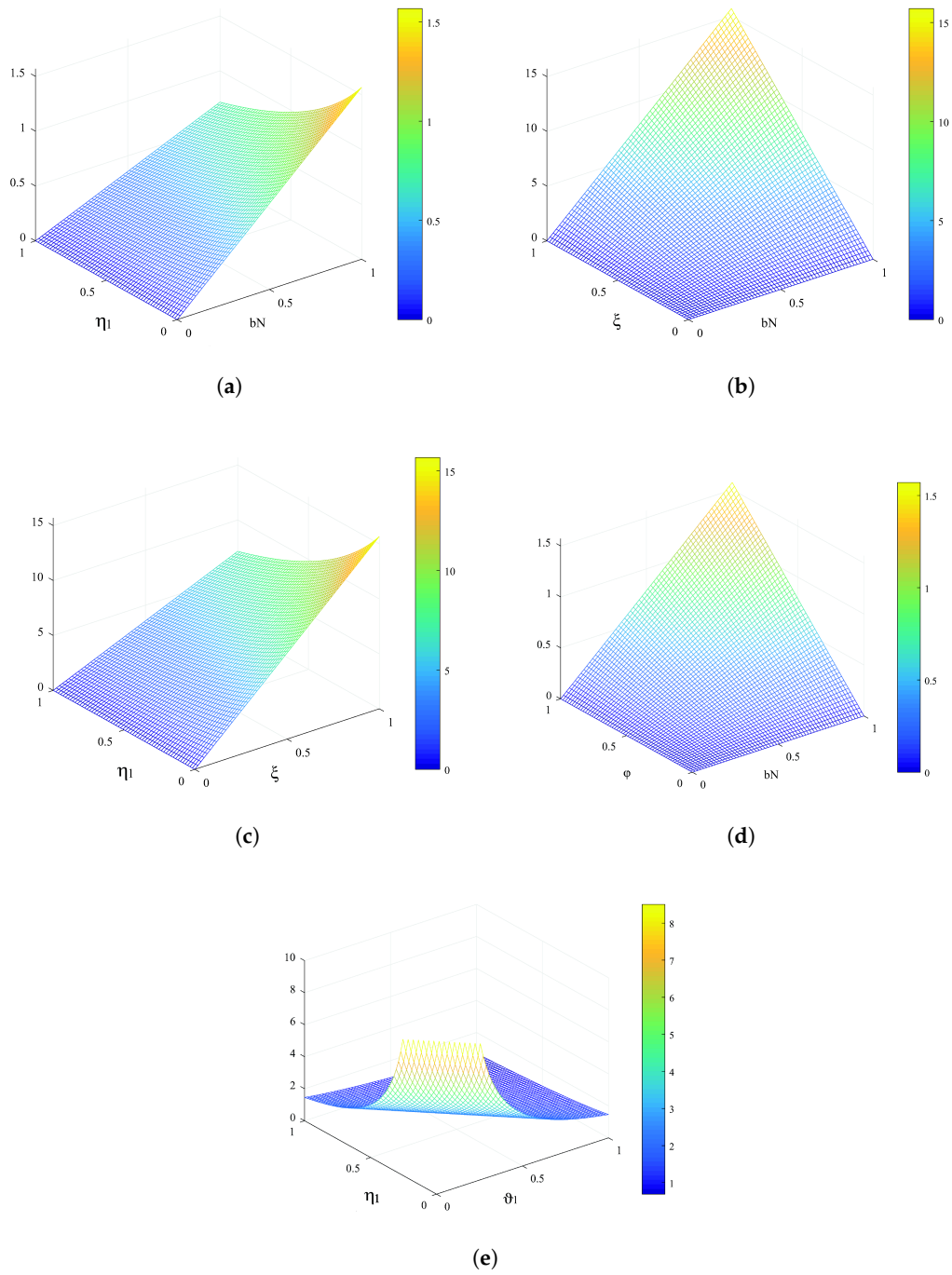


Figure 1. Cont.

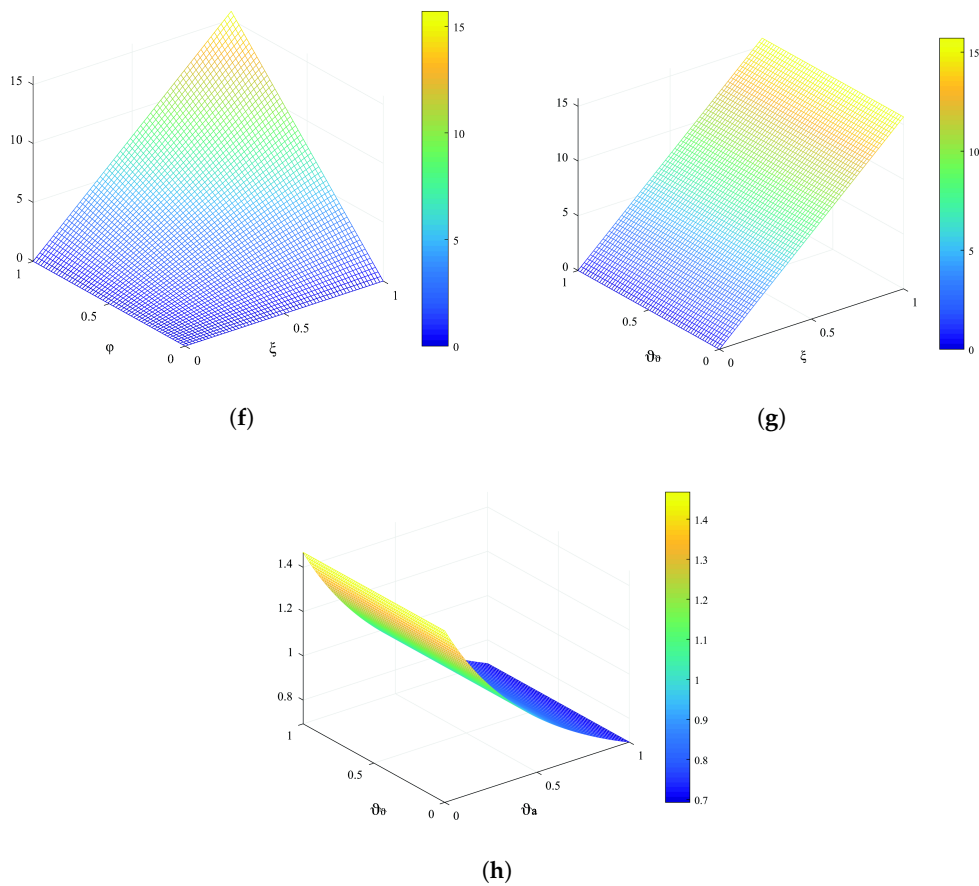


Figure 1. The graphs display the results of a sensitivity analysis on the basic reproductive number R_0 . (a) R_0 with η_1, bN ; (b) R_0 with ζ, bN ; (c) R_0 with η_1, ζ ; (d) R_0 with φ, bN ; (e) R_0 with η_1, ϑ_1 ; (f) R_0 with φ, ζ ; (g) R_0 with ϑ_θ, ζ ; (h) R_0 with $\vartheta_\theta, \vartheta_a$.

4. Equilibria Points

The aforementioned system (1) has two possible equilibria: one is the disease-free equilibrium (DFE) and second one is the endemic equilibrium (EE). The DFE, denoted by \mathcal{F}_0 , is given by $\mathcal{F}_0 = \left(\frac{bN}{\eta_0}, 0, 0, 0, 0, 0 \right)$. The EE, denoted by \mathcal{F}_1 , is found by setting “ $S = S_*, E = E_*, I = I_*, A = A_*, H = H_*$, and $\mathcal{R} = \mathcal{R}_*$, and the LHS of the resulting system to zero”. We obtain the following expression after simplification, S_*, E_*, I_*, A_*, H_* , and \mathcal{R}_* at the EE.

$$\begin{aligned}
 S_* &= \frac{NbNQ_2}{\varphi Q_2 + \varphi q \vartheta_a + \eta_0 N Q_2}, \\
 E_* &= \frac{NbNQ_2 + \varphi q \vartheta_a + NbNQ_2}{\varphi Q_2 + \varphi q \vartheta_a + \eta_0 N Q_2}, \\
 I_* &= \frac{(\chi \zeta)(NbNQ_2 + (R_0 - 1) + NbNQ_2)}{Q_3 \varphi + \varphi q \vartheta_a + \eta_0 N Q_2}, \\
 A_* &= \frac{\chi(1 - \zeta)NbNQ_2^2 + \varphi q \vartheta_a + NbNQ_2}{\varphi Q_2 + \varphi q \vartheta_a + \eta_0 N Q_3}, \\
 H_* &= \frac{\vartheta_a I_*}{Q_2}, \\
 \mathcal{R}_* &= \frac{Q_2 I_* + Q_1}{Q_2}.
 \end{aligned}
 \tag{3}$$

4.1. Local Stability

We show the local asymptotic stability (LAS) of the DFE as well as the EE of the system (1) with the help of the following theorem.

Theorem 1. *If the basic reproductive number R_0 is less than 1, the DFE point is LAS.*

Proof. To show the local stability of the system, about the point DFE, the Jacobian matrix for the said system (1) is

$$J_0 = \begin{pmatrix} -\eta_0 & 0 & -\frac{\varphi S_0}{N} & 0 & \frac{\varphi q S_0}{N} & 0 \\ 0 & -(\chi + \eta_0) & \frac{\varphi S_0}{N} & 0 & \frac{\varphi q S_0}{N} & 0 \\ 0 & \chi \xi & -Q_3 & 0 & 0 & 0 \\ 0 & \chi(1 - \xi) & 0 & -\eta_2 & 0 & 0 \\ 0 & 0 & \vartheta_a & 0 & -Q_2 & 0 \\ 0 & 0 & \vartheta_1 & 0 & \vartheta_\theta & -\eta_0 \end{pmatrix}. \tag{4}$$

By conducting a row operation, reducing the matrix to echelon form, the following Jacobian matrix is obtained

$$\begin{pmatrix} -\eta_0 & 0 & -\frac{\varphi S_0}{N} & 0 & \frac{\varphi q S_0}{N} & 0 \\ 0 & -(\chi + \eta_0) & \frac{\varphi S_0}{N} & 0 & \frac{\varphi q S_0}{N} & 0 \\ 0 & 0 & \mathbf{A} & \frac{\varphi q S_0 \chi \xi}{N} & 0 & \frac{\varphi q S_0 \chi \xi}{N} \\ 0 & 0 & 0 & \mathbf{B} & \frac{\varphi q S_0 \chi}{N} & 0 \\ 0 & 0 & 0 & 0 & \mathbf{C} & 0 \\ 0 & 0 & 0 & 0 & 0 & \mathbf{D} \end{pmatrix}, \tag{5}$$

$$\begin{aligned} \mathbf{A} &= -Q_3 Q_2 (\chi + \eta_0) - \frac{\varphi S_0 \chi \xi}{N}, \\ \mathbf{B} &= -(\eta_0 + \eta_2) (\chi + \eta_0) Q_1 - \frac{\varphi S_0 \chi \xi}{N}, \\ \mathbf{C} &= -Q_1 Q_2 Q_3 (S_0 + \eta_0), \\ \mathbf{D} &= -\eta_0 Q_3 (\kappa + \eta_0) - \frac{(\varphi S_0 \chi \xi)}{N} - [(1 - R_0) (N(\chi + \eta_0) Q_2 Q_3) \varphi q S_0 \chi \xi]. \end{aligned}$$

According to [42], when $R_0 < 1$, the matrices \mathbf{A} , \mathbf{B} , \mathbf{C} , and \mathbf{D} are all negative, and the eigenvalues have negative real parts. As a result, the DFE is LAS. \square

Theorem 2. *If R_0 is greater than 1, the EE point is LAS.*

Proof. Consider the Jacobian of the considered problem (1) at \mathcal{F}_1 is,

$$J_0 = \begin{pmatrix} -\frac{\varphi \mathcal{I}_*}{N} - \frac{\varphi \mathcal{H}_* q}{N} - \eta_0 & 0 & -\frac{\varphi S_*}{N} & 0 & -\frac{\varphi q S_*}{N} & 0 \\ \frac{\varphi \mathcal{I}_*}{N} + \frac{\varphi \mathcal{H}_* q}{N} & -(\chi + \eta_0) & \frac{\varphi S_*}{N} & 0 & \frac{\varphi q S_*}{N} & 0 \\ 0 & \chi \xi & Q_3 & 0 & 0 & 0 \\ 0 & \chi(1 - \xi) & 0 & -(\eta_0 + \eta_1) & 0 & 0 \\ 0 & 0 & \vartheta_a & 0 & -(\vartheta_\theta + \eta_0) & 0 \\ 0 & 0 & \vartheta_1 & 0 & \vartheta_\theta & -\eta_0 \end{pmatrix}. \tag{6}$$

After performing a row operation and simplifying the resulting expressions, we obtain the following Jacobian matrix:

$$\begin{pmatrix} -\frac{\varphi \mathcal{I}_*}{N} - \frac{\varphi \mathcal{H}_* q}{N} - \eta_0 & 0 & -\frac{\varphi S_*}{N} & 0 & -\frac{\varphi q S_*}{N} & 0 \\ 0 & -(\chi + \eta_0) \left(\frac{\varphi \mathcal{I}_*}{N} + \frac{\varphi \mathcal{H}_* q S_*}{N} + \eta_0 \right) & -\frac{\varphi S_*}{N} & 0 & -\frac{\varphi q S_*}{N} & 0 \\ 0 & 0 & \mathbb{Z}_1 & \eta_2 \xi & 0 & 0 \\ 0 & 0 & 0 & \mathbb{Z}_2 & \mathbb{Z}_3 & \mathbb{Z}_4 \\ 0 & 0 & 0 & 0 & \mathbb{Z}_5 & \eta_0 \vartheta_\theta \\ 0 & 0 & 0 & 0 & 0 & \mathbb{Z}_6 \end{pmatrix}, \tag{7}$$

where

$$\begin{aligned} \mathbb{Z}_1 &= -\zeta Q_3, \\ \mathbb{Z}_2 &= -\eta_2(\kappa + \eta_0)(\varphi \mathcal{I}_* + \varphi q \mathcal{H}_* + \eta_0) \vartheta_1, \\ \mathbb{Z}_3 &= -\vartheta_\vartheta \varphi \mathcal{S}_* \eta_0 \chi \zeta, \\ \mathbb{Z}_4 &= -\eta_0 \varphi \mathcal{S}_* \chi (1 - \zeta), \\ \mathbb{Z}_5 &= -Q_2 \vartheta_1 - \vartheta_a - \vartheta_\vartheta, \\ \mathbb{Z}_6 &= -\eta_0 Q_3 (\eta_2 (\chi + \eta_0) (\varphi \mathcal{I}_* \\ &+ \varphi q \mathcal{H}_* + \eta_0) \vartheta_1 (\mathbf{R}_0 - 1) \times [(\chi + \eta_0) Q_3] (\varphi \mathcal{S}_* \eta_0 \varphi (\eta_2 \zeta \vartheta_1) (\vartheta_\vartheta + \eta_0) \vartheta_1 + \vartheta_a \\ &+ Q_3 (\eta_0 \zeta Q_3 (\eta_2 (\chi + \eta_0)) (\varphi \mathcal{I}_* + \varphi q \mathcal{H}_* + \eta_0) \vartheta_1 \\ &+ (\vartheta_\vartheta \varphi \mathcal{S}_* \eta_0 \chi \zeta) \eta_2 \zeta \vartheta_1). \end{aligned}$$

The eigenvalues are given by

$$\begin{aligned} \zeta_1 &= -\frac{\varphi \mathcal{I}_*}{\mathbf{N}} - \frac{\varphi \mathcal{H}_* q}{\mathbf{N}} - \eta_0 < 0, \\ \zeta_2 &= -(\chi + \eta_0) \left(\frac{\varphi \mathcal{I}_*}{\mathbf{N}} + \frac{\varphi \mathcal{H}_* q \mathcal{S}_*}{\mathbf{N}} + \eta_0 \right) < 0, \\ \zeta_3 &= -\zeta (\vartheta_a + \vartheta_1 + \eta_0 + \eta_1) = \mathbb{Z}_1 < 0, \\ \zeta_4 &= -\eta_2 (\kappa + \eta_0) (\varphi \mathcal{I}_* + \varphi q \mathcal{H}_* + \eta_0) \vartheta_1 = \mathbb{Z}_2 < 0, \\ \zeta_5 &= -(\vartheta_\vartheta + \eta_0) \vartheta_1 - \vartheta_a - \vartheta_\vartheta = \mathbb{Z}_5 < 0, \\ \zeta_6 &= \mathbb{Z}_6 < 0. \end{aligned} \tag{8}$$

As per the findings reported in [43], when $\mathbf{R}_0 > 1$, all of the eigenvalues have nonpositive real parts, which indicates that the EE point is LAS. \square

4.2. Analysis of Global Stability

The next theorem presents that the said system is globally asymptotically stable (GAS) for the DFE and EE point.

Theorem 3. *The DFE of the system is GAS for $\mathbf{R}_0 < 1$, otherwise unstable.*

Proof. We define the Lyapunov function as follows:

$$U(t) = k_1 (\mathcal{S} - \mathcal{S}_0) + k_2 \mathcal{E} + k_3 \mathcal{I} + k_4 \mathcal{A} + k_5 \mathcal{H}. \tag{9}$$

We differentiate Equation (9) and obtain:

$$U'(t) = k_1 \mathcal{S}' + k_2 \mathcal{E}' + k_3 \mathcal{I}' + k_4 \mathcal{A}' + k_5 \mathcal{H}'. \tag{10}$$

Using model (1), we obtain

$$\begin{aligned}
 U'(t) &= \kappa_1[bN - \frac{\varphi \mathcal{I} \mathcal{S}}{N} - \frac{\varphi q \mathcal{H} \mathcal{S}}{N} - \eta_0 \mathcal{S}] + \kappa_2[\frac{\varphi \mathcal{I} \mathcal{S}}{N} + \frac{\varphi q \mathcal{H} \mathcal{S}}{N} - (\chi + \eta_0) \mathcal{E}] \\
 &+ \kappa_3[\chi \xi \mathcal{E} - (\vartheta_a + \vartheta_1) \mathcal{I} - (\eta_0 + \eta_1) \mathcal{I}] + \kappa_4[\chi(1 - \xi) \mathcal{E} - (\eta_0 + \eta_2) \mathcal{A}] \\
 &+ \kappa_5[\vartheta_a \mathcal{I} - \vartheta_\theta \mathcal{H} - \eta_0 \mathcal{H}].
 \end{aligned}$$

If we choose the positive parameter values $\kappa_1 = \kappa_2 = \kappa_4 = \xi$, $\kappa_3 = 1$, and $\kappa_5 = q\varphi\rho$, and simplify, we obtain:

$$\begin{aligned}
 U'(t) &= -\xi\eta_0(\mathcal{S} - \mathcal{S}_0) - 2\frac{\varphi q \mathcal{H} \mathcal{S}}{N} - Q_1 \xi \eta_0 \mathcal{E} - (\eta_0 + \eta_2) \mathcal{A} \\
 &- Q_3[1 - \mathbf{R}_0] - Q_2 Q_3(\kappa + \eta_0) - Q_2^2 \mathcal{H}.
 \end{aligned}$$

where

$$\mathcal{S}_0 = \frac{bN}{\eta_0},$$

Let $U'(t)$ be a function of time t , and let \mathcal{S} and \mathbf{R}_0 be constants. If $\mathcal{S} > \mathcal{S}_0$ and $\mathbf{R}_0 < 1$, then $U'(t)$ is negative. If $\mathcal{S} = \mathcal{S}_0$, then $U'(t) = 0$. According to the LaSalle invariance principle [44,45], if $\mathcal{E} = \mathcal{I} = \mathcal{A} = \mathcal{H} = 0$, then the set of initial conditions for which $U'(t)$ approaches zero as t approaches infinity is an invariant set.

Therefore, the DFE \mathcal{F}_0 is GAS. \square

Theorem 4. When $\mathbf{R}_0 > 1$, the EE point is GAS at \mathcal{F}_1 , and unstable when $\mathbf{R}_0 < 1$.

Proof. For the GAS of the EE point, we define the Lyapunov function as:

$$U(t) = \frac{1}{2}[p_1(\mathcal{S} - \mathcal{S}_*) + p_2(\mathcal{E} - \mathcal{E}_*) + p_3(\mathcal{I} - \mathcal{I}_*) + p_4(\mathcal{A} - \mathcal{A}_*) + p_5(\mathcal{H} - \mathcal{H}_*)]^2, \tag{11}$$

and we introduce the constants p_1, p_2, p_3, p_4 , and p_5 , which will be chosen later. Upon differentiating Equation (11), we obtain:

$$\begin{aligned}
 U'(t) &= [p_1(\mathcal{S} - \mathcal{S}_*) + p_2(\mathcal{E} - \mathcal{E}_*) + p_3(\mathcal{I} - \mathcal{I}_*) + p_4(\mathcal{A} - \mathcal{A}_*) \\
 &+ p_5(\mathcal{H} - \mathcal{H}_*)][p_1(\frac{d\mathcal{S}}{dt}) + p_2(\frac{d\mathcal{E}}{dt}) + p_3(\frac{d\mathcal{I}}{dt}) + p_4(\frac{d\mathcal{A}}{dt}) + p_5(\frac{d\mathcal{H}}{dt})],
 \end{aligned}$$

$$\begin{aligned}
 U'(t) &= p_1(\mathcal{S} - \mathcal{S}_*) + p_2(\mathcal{E} - \mathcal{E}_*) + p_3(\mathcal{I} - \mathcal{I}_*) + p_4(\mathcal{A} - \mathcal{A}_*) + p_5(\mathcal{H} - \mathcal{H}_*)(p_1(bN - \frac{\varphi \mathcal{I} \mathcal{S}}{N} - \frac{\varphi q \mathcal{H} \mathcal{S}}{N} - \eta_0 \mathcal{S}) \\
 &+ p_2(\frac{\varphi \mathcal{I} \mathcal{S}}{N} + \frac{\varphi q \mathcal{H} \mathcal{S}}{N} - (\chi + \eta_0) \mathcal{E} + p_3[\chi \xi \mathcal{E} - (\vartheta_a + \vartheta_1) \mathcal{I} - (\eta_0 + \eta_1) \mathcal{I}] + p_4[\chi(1 - \xi) \mathcal{E} - (\eta_0 + \eta_2) \mathcal{A}] \\
 &+ p_5(\vartheta_a \mathcal{I} - \vartheta_\theta \mathcal{H} - \eta_0 \mathcal{H}).
 \end{aligned}$$

After some calculation, we obtain, and utilizing the values of p_1, \dots, p_5 , we obtain

$$U'(t) = -\frac{(\varphi \mathcal{S}_*)}{N}(\mathcal{S} - \mathcal{S}_*) - (\mathbf{R}_0 - 1)Q_1 Q_2 - \frac{\varphi q \mathcal{H}_* \mathcal{S}_*}{N}[\mathcal{E} + \mathcal{I} + \mathcal{A}] - (\vartheta_a \mathcal{I} - \vartheta_\theta)Q_2 Q_3^2 \mathcal{H}_*$$

For $\mathcal{S} = \mathcal{S}_*$ and $(\vartheta_a > \vartheta_\theta)$ for \mathbf{R}_0 is greater than 1; thus, the proof is finished. \square

5. Results and Discussion

In this context, we substantiate our analytical discoveries through the application of the fourth-order Runge–Kutta method [46]. We select certain parameters for illustrative purposes, while obtaining others from published data sources [38]. The parameters employed in the simulation are chosen with careful consideration of their biological plausibility. The ensuing

set of parameters is utilized for the subsequent analysis. $\varphi = 0.007; q = 0.003; \chi = 0.005; \xi = 0.0001; \eta_0 = 0.0003; \eta_1 = 0.0001; \zeta = 0.002; \vartheta_1 = 0.001; \vartheta_a = 0.000001; \vartheta_\theta = 0.0007; \text{ and } bN = 0.00004$. To validate the analytical findings of the proposed model concerning the DFE, we employed the aforementioned parameter values. Subsequently, we computed the DFE point's coordinates and the threshold parameter \mathbf{R}_0 as $(7.98337196, 0, 0, 0, 0)$ and (0.043732) , respectively. The simulation outcomes utilizing the aforementioned parameters are depicted in Figures 2 and 3, thereby substantiating the analytical conclusions outlined in the theorem. To corroborate this, we employed the linear stability analysis technique and introduced perturbations to the initial compartmental population values. Remarkably, these perturbed values consistently converged to the DFE, underscoring its robustness against varying initial conditions, $S(0) = 1000, \mathcal{E}(0) = 800, \mathcal{I}(0) = 600, \mathcal{A}(0) = 500, \mathcal{H}(0) = 400,$ and $\mathcal{R}(0) = 300$. Drawing from the theoretical interpretation of the data, a definitive conclusion can be drawn: when the value of \mathbf{R}_0 is below 1, the disease transmission will inevitably diminish over time. This is evidenced by the convergence of every solution curve to a stable position, as depicted in the corresponding plots.

$$\begin{aligned} \frac{S^{i+1} - S^i}{l} &= bN - \frac{\varphi \mathcal{I}^i S^{i+1}}{N} - \frac{\varphi q \mathcal{H}^i S^{i+1}}{N} - \eta_0 S^{i+1}, \\ \frac{\mathcal{E}^{i+1} - \mathcal{E}^i}{l} &= \frac{\varphi \mathcal{I}^i S^{i+1}}{N} + \frac{\varphi q \mathcal{H}^i S^{i+1}}{N} - (\chi + \eta_0) \mathcal{E}^{i+1}, \\ \frac{\mathcal{I}^{i+1} - \mathcal{I}^i}{l} &= \chi \xi \mathcal{E}^{i+1} - (\vartheta_a + \vartheta_1) \mathcal{I}^{i+1} - (\eta_0 + \eta_1) \mathcal{I}^{i+1}, \\ \frac{\mathcal{A}^{i+1} - \mathcal{A}^i}{l} &= \chi(1 - \xi) \mathcal{E}^{i+1} - (\eta_0 + \eta_2) \mathcal{A}^{i+1}, \\ \frac{\mathcal{H}^{i+1} - \mathcal{H}^i}{l} &= \vartheta_a \mathcal{I}^{i+1} - \vartheta_\theta \mathcal{H}^{i+1} - \eta_0 \mathcal{H}^{i+1}, \\ \frac{\mathcal{R}^{i+1} - \mathcal{R}^i}{l} &= \vartheta_1 \mathcal{I}^{i+1} + \vartheta_\theta \mathcal{H}^{i+1} - \eta_0 \mathcal{R}^{i+1}. \end{aligned}$$

Used Algorithm

Step 1: $(S_0, \mathcal{E}_0, \mathcal{I}_0, \mathcal{A}_0, \mathcal{H}_0, \mathcal{R}_0 = 0)$.

Step 2: Let $i = 1, 2, \dots, n - 1$.

$$\begin{aligned} S^{i+1} &= \frac{Nlb}{\varphi \mathcal{I}^i S^{i+1} + \varphi q \mathcal{H}^i S^{i+1} l + \eta_0 l N} + \frac{S^{i+1}}{\varphi \mathcal{I}^i S^{i+1} + \varphi q \mathcal{H}^i S^{i+1} l + \eta_0 l N}, \\ \mathcal{E}^{i+1} &= \frac{l \varphi \mathcal{I}^i S^{i+1}}{N(1 + l(\chi + \eta_0))} + \frac{l \varphi q \mathcal{H}^i S^{i+1}}{N(1 + l(\chi + \eta_0))} + \frac{\mathcal{E}^{i+1}}{(1 + l(\chi + \eta_0))}, \\ \mathcal{I}^{i+1} &= \frac{l \chi \xi \mathcal{E}^{i+1}}{(1 + l(\vartheta_a + \vartheta_1) + (\eta_0 + \eta_1)l)} + \frac{\mathcal{I}^{i+1}}{1 + l(\vartheta_a + \vartheta_1) + (\eta_0 + \eta_1)l}, \\ \mathcal{A}^{i+1} &= \frac{l \chi(1 - \xi) \mathcal{E}^{i+1}}{1 + (\eta_0 + \eta_2)l} + \frac{\mathcal{A}^{i+1}}{1 + (\eta_0 + \eta_2)l}, \\ \mathcal{H}^{i+1} &= \frac{l \vartheta_a \mathcal{I}^{i+1}}{1 + \eta_0 l + \vartheta_\theta l} + \frac{\mathcal{H}^{i+1}}{1 + \vartheta_\theta + \eta_0 l}, \\ \mathcal{R}^{i+1} &= \frac{l \vartheta_1 \mathcal{I}^{i+1}}{1 + \eta_0 l} + \frac{l \vartheta_\theta \mathcal{H}^{i+1}}{1 + \eta_0 l} + \frac{\mathcal{R}^{i+1}}{1 + \eta_0 l}. \end{aligned}$$

Step 3: Let $i = 1, 2, 3, \dots, n - 1$, by letting “ $S_*(t_i) = S_*, \mathcal{E}_*(t_i) = \mathcal{E}_*, \mathcal{I}_*(t_i) = \mathcal{I}_*, \mathcal{A}_*(t_i) = \mathcal{A}_*, \mathcal{H}_*(t_i) = \mathcal{H}_*, \mathcal{R}_*(t_i) = \mathcal{R}_*$.”

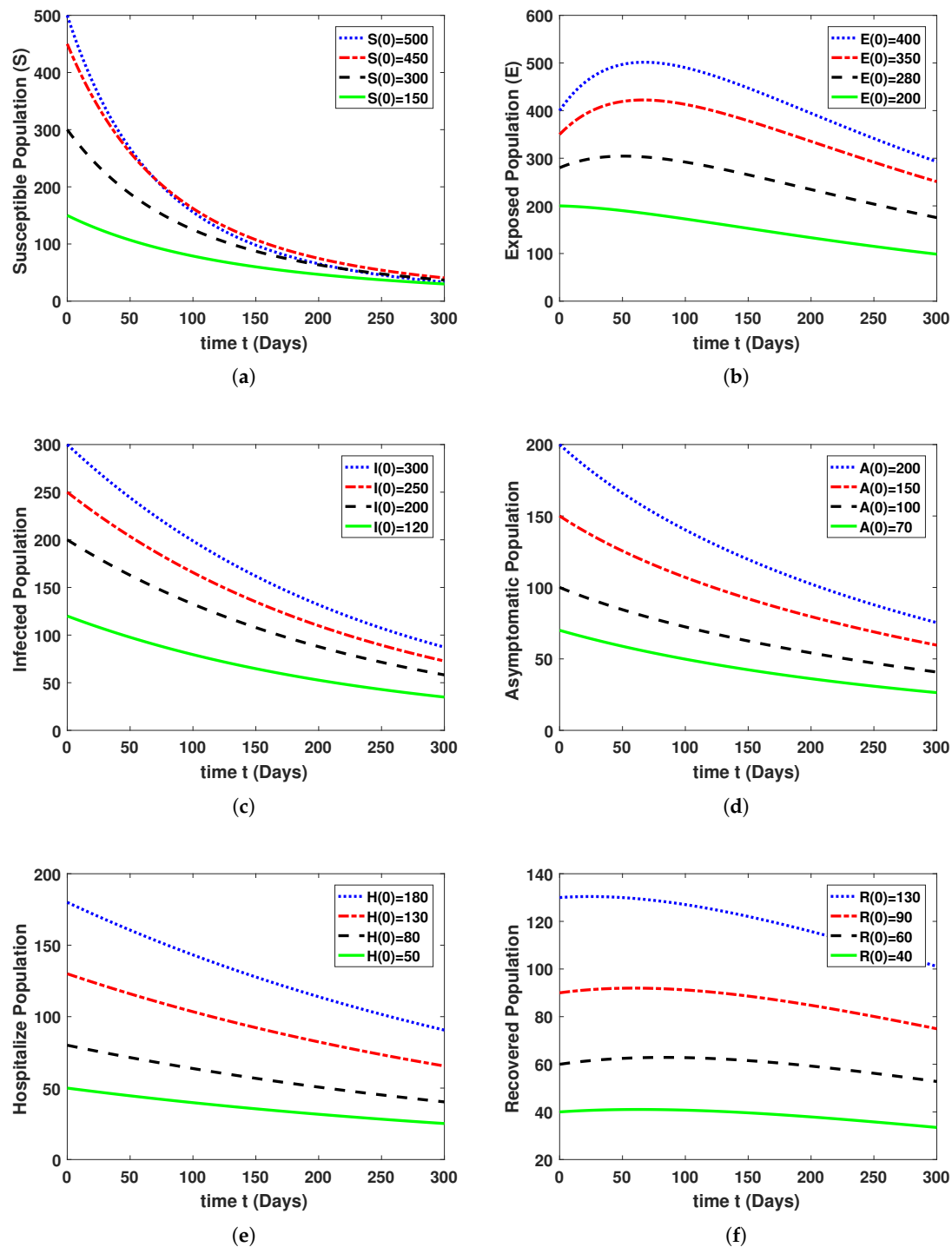


Figure 2. The time dynamics of the compartmental populations in model (1) are shown graphically for an initial population value. (a) Class of S ; (b) class of \mathcal{E} ; (c) class of \mathcal{I} ; (d) class of \mathcal{A} ; (e) class of \mathcal{H} ; (f) class of \mathcal{R} .

Subsequently, we proceed to explore the system’s dynamics around the EE by assuming an alternate set of parameters: $\varphi = 0.17$, $q = 0.03$, $\chi = 0.05$, $\zeta = 0.01$, $\eta_0 = 0.03$, $\eta_1 = 0.031$, $\xi = 0.052$, $\vartheta_1 = 0.041$, $\vartheta_a = 0.000001$, $\vartheta_\theta = 0.0007$, and $bN = 0.004$. Using these parameter values acquired earlier, we calculate the endemic equilibrium points and the associated R_0 for the model (1). When $R_0 > 1$, the endemic equilibrium point is determined to be (40.76549, 110.908700, 70.45321, 85.934214, 85.7659321, 120.7659321),

with a calculated value of $R_0 = 7.13587$. Assuming the same initial population sizes for the compartments as in the previous analysis, the graphical results indicate that the populations of susceptible, exposed, infected asymptomatic, hospitalized, and recovered individuals initially undergo fluctuations before eventually stabilizing at their respective equilibrium values. For the parameter values employed in this study, the equilibrium point is $(24.76549, 99.908700, 22.45321, 90.934214, 85.7659321, 120.7659321)$.

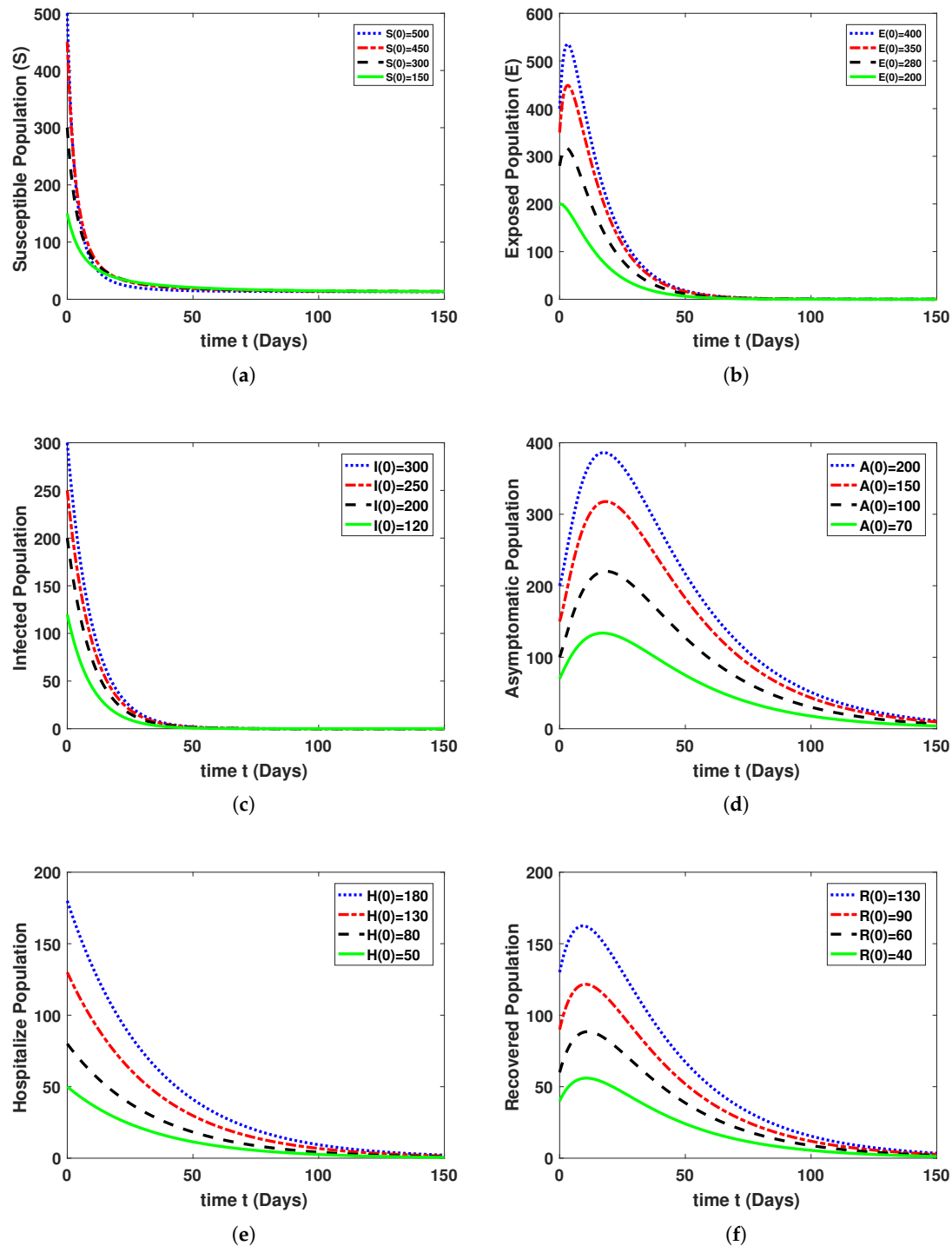


Figure 3. The time dynamics of the compartmental populations in model (1) are shown graphically for initial population values. (a) Class of \mathcal{S} ; (b) class of \mathcal{E} ; (c) class of \mathcal{I} ; (d) class of \mathcal{A} ; (e) class of \mathcal{H} ; (f) class of \mathcal{R} .

6. Analysis of Optimal Control

Here, we aim to establish an effective control strategy to prevent the spread of MERS in the population. Optimal control theory is a powerful mathematical technique that can be applied to design control schemes for a variety of infectious diseases. To achieve this, we apply optimal control theory, as described in previous works [46–49], to establish an appropriate control strategy. Our objective in this study is to reduce the prevalence of MERS in the populace by increasing the number of persons who recover from the disease, denoted as \mathcal{R} , and decreasing the number of individuals who are infectious, denoted as \mathcal{I} , and hospitalized, denoted as \mathcal{H} , by implementing time-dependent control variables such as treatment $v_1(t)$ and care $v_2(t)$. In model (1), we take six state variables \mathcal{S} , \mathcal{E} , \mathcal{I} , \mathcal{A} , \mathcal{H} , and \mathcal{R} . Now, for the control problem, we take the two control variables, that is treatment $v_1(t)$ and care $v_2(t)$. Hence, we have the successive optimal control problem to reduce the objective functional

$$J(v_1, v_2) = \int_0^T [c_1\mathcal{I}(t) + c_2\mathcal{H}(t) + \frac{1}{2}(c_3v_1^2(t) + c_4v_2^2(t))]dt \tag{12}$$

subject to

$$\begin{aligned} \dot{\mathcal{S}}(t) &= bN - \frac{\varphi\mathcal{I}\mathcal{S}}{N} - \frac{\varphi q\mathcal{H}\mathcal{S}}{N} - \eta_0\mathcal{S}, \\ \dot{\mathcal{E}}(t) &= \frac{\varphi\mathcal{I}\mathcal{S}}{N} + \frac{\varphi q\mathcal{H}\mathcal{S}}{N} - (\chi + \eta_0)\mathcal{E}, \\ \dot{\mathcal{I}}(t) &= \chi\xi\mathcal{E} - (\vartheta_a + \vartheta_1)\mathcal{I} - (\eta_0 + \eta_1) - v_1\mathcal{I}, \\ \dot{\mathcal{A}}(t) &= \chi(1 - \xi)\mathcal{E} - (\eta_0 + \eta_2)\mathcal{A}, \\ \dot{\mathcal{H}}(t) &= \vartheta_a\mathcal{I} - \vartheta_\theta\mathcal{H} - \eta_0\mathcal{H} - v_2\mathcal{H}, \\ \dot{\mathcal{R}}(t) &= \vartheta_1\mathcal{I} + \vartheta_\theta\mathcal{H} - \eta_0\mathcal{R} + v_1\mathcal{I} + v_2\mathcal{H}, \end{aligned} \tag{13}$$

with initial conditions

$$“\mathcal{S}(0) \geq 0, \mathcal{E}(0) \geq 0, \mathcal{I}(0) \geq 0, \mathcal{A}(0) \geq 0, \mathcal{H}(0) \geq 0, \mathcal{R}(0) \geq 0”.$$

Equation (12) includes weight constants c_1, c_2, c_3 , and c_4 that correspond to the relative importance of infected people I and hospitalized individual H in the objective function. The parameters $\frac{1}{2}c_3v_1^2$ and $\frac{1}{2}c_4v_2^2$ represent the costs associated with self-care and treatment. The primary objective is to evaluate the control function to achieve a specific goal.

$$J(v_1^*, v_2^*) = \min\{J(v_1, v_2), v_1, v_2 \in U\} \tag{14}$$

dependent on control system (13), where U in Equation (14) is known as the control set and is presented as,

$$“U = \{(v_1, v_2) / v_i(t) \text{ is Lebesgue measurable on } [0, 1], 0 \leq v_i(t) \leq 1, i = 1, 2\}.” \tag{15}$$

Before proceeding, it is important to establish the existence of control variables. According to Kamien and Aldila’s study [47], a solution for a state system can be found when the controls are bounded and Lebesgue measurable, in addition to satisfying the initial conditions. Thus, we can suppose that the considered control model can be formulated in the manner presented below.

$$\frac{d\phi}{dt} = \mathcal{A}\phi + \mathcal{B}\phi.$$

From the above equation $\phi = (S, \mathcal{E}, \mathcal{I}, \mathcal{A}, \mathcal{H}, \mathcal{R})$, where $\mathcal{A}(\phi)$ and $\mathcal{B}(\phi)$ denote the linear and nonlinear bounded coefficient \ni

$$J_0 = \begin{pmatrix} -\eta_0 & 0 & 0 & 0 & 0 & 0 \\ 0 & -(\chi + \eta_0) & 0 & 0 & 0 & 0 \\ 0 & \chi\xi & -Q_3 & 0 & 0 & 0 \\ 0 & \chi(1 - \xi) & 0 & -\eta_2 & 0 & 0 \\ 0 & 0 & \vartheta_a & 0 & -Q_2 & 0 \\ 0 & 0 & \vartheta_1 & 0 & \vartheta_\theta & -\eta_0 \end{pmatrix}. \tag{16}$$

$$B(\phi) = \begin{pmatrix} bN - \frac{\varphi\mathcal{I}\mathcal{S}}{N} - \frac{\varphi q\mathcal{H}\mathcal{S}}{N} \\ \frac{\varphi\mathcal{I}\mathcal{S}}{N} + \frac{\varphi q\mathcal{H}\mathcal{S}}{N} \\ 0 \\ 0 \\ 0 \\ 0 \end{pmatrix}. \tag{17}$$

Letting $L(\phi) = \mathcal{A}\phi + FCE$,

$$\begin{aligned} |F(\phi_1) - F(\phi_2)| &\leq m_1|S_1 - S_2| + m_2|\mathcal{E}_1 - \mathcal{E}_2| + m_3|\mathcal{I}_1 - \mathcal{I}_2| + m_4|\mathcal{A}_1 - \mathcal{A}_2| + m_5|\mathcal{H}_1 - \mathcal{H}_2| + m_6|\mathcal{R}_1 - \mathcal{R}_2| \\ &\leq N|S_1 - S_2| + |\mathcal{E}_1 - \mathcal{E}_2| + |\mathcal{I}_1 - \mathcal{I}_2| + |\mathcal{A}_1 - \mathcal{A}_2| + |\mathcal{H}_1 - \mathcal{H}_2| + |\mathcal{R}_1 - \mathcal{R}_2|. \end{aligned}$$

Here, $N = \max(m_1, m_2, m_3, m_4, m_5, m_6)$ is a constant that is independent of the state variables in the aforementioned system. We also express

$$|L(\phi_1) - L(\phi_2)| \leq M|(\phi_1) - (\phi_2)|.$$

The solution for (13) exists due to the nonnegativity of the model state variables $S, \mathcal{E}, \mathcal{I}, \mathcal{A}, \mathcal{H}$, and \mathcal{R} . Furthermore, it has been shown that the function L is Lipschitz uniformly continuous, and where $M = (N, \|\mathcal{K}\|) < \infty$. Based on the properties mentioned earlier, we present the following theorem to establish the existence of a solution for model (1), which we then proceed to prove.

Theorem 5. For the control problem in Equations (12) and (13) there exists an optimal control as $v^* = (v_1^*, v_2^*) \in U$.

Proof. It is evident that the control and state variables in system (1) are positive. Additionally, the control variables set U is a closed and convex set, as mentioned in the problem statement. Furthermore, the control system is bounded, implying the compactness of the system. The integral in the objective function of the optimization problem, given by $c_1\mathcal{I} + c_2\mathcal{H} + \frac{1}{2}(c_3v_1^2(t) + c_4v_2^2(t))$, is also convex w.r.t the control set U . This convexity guarantees the existence results for optimal control for the optimal control variables (v_1^*, v_2^*) . \square

6.1. Methods

Next to show the optimal solution to the control model (12) and (13), we can apply the Lagrangian and Hamiltonian methods, described in the equation below

$$L(\mathcal{I}, \mathcal{H}, v_1, v_2) = c_1\mathcal{I} + c_2\mathcal{H} + \frac{1}{2}(c_3v_1^2(t) + c_4v_2^2(t)).$$

To describe the Hamiltonian (\mathcal{H}), by utilizing the notation $\vartheta = (\vartheta_1, \vartheta_2, \vartheta_3, \vartheta_4, \vartheta_5, \vartheta_6)$ and $y = (y_1, y_2, y_3, y_4, y_5, y_6)$, thus

$$\mathcal{H}(x, v, \vartheta) = L(x, v) + \vartheta Z(x, v),$$

where

$$\begin{aligned}
 Z_1 &= bN - \frac{\varphi \mathcal{I} \mathcal{S}}{N} - \frac{\varphi q \mathcal{H} \mathcal{S}}{N} - \eta_0 \mathcal{S}, \\
 Z_2 &= \frac{\varphi \mathcal{I} \mathcal{S}}{N} + \frac{\varphi q \mathcal{H} \mathcal{S}}{N} - (\chi + \eta_0) \mathcal{E}, \\
 Z_3 &= \chi \zeta \mathcal{E} - (\vartheta_a + \vartheta_1) \mathcal{I} - (\eta_0 + \eta_1) - v_1(t) \mathcal{I}(t), \\
 Z_4 &= \chi(1 - \zeta) \mathcal{E} - (\eta_0 + \eta_2) \mathcal{A}, \\
 Z_5 &= \vartheta_a \mathcal{I} - \vartheta_\vartheta \mathcal{H} - \eta_0 \mathcal{H} - v_2(t) \mathcal{H}(t), \\
 Z_6 &= \vartheta_1 \mathcal{I} + \vartheta_\vartheta \mathcal{H} - \eta_0 \mathcal{R} + v_1(t) \mathcal{I}(t) + v_2(t) \mathcal{H}(t),
 \end{aligned}
 \tag{18}$$

Thus we apply the Pontryagin Maximum Principle [50,51] to the Hamiltonian in order to determine the optimal solution. According to this principle, if (x^*, v^*) is an optimal solution, then there must exist a function $\vartheta \ni$:

$$\begin{aligned}
 \frac{dx}{dt} &= \frac{\partial \mathcal{H}}{\partial \vartheta}, 0 = \frac{\partial \mathcal{H}}{\partial u}, \\
 \vartheta(t)' &= -\frac{\partial \mathcal{H}}{\partial x}.
 \end{aligned}$$

$$\mathcal{H}(t, x^*, v^*, \vartheta) \partial x = \max_{v_1, v_2, v_3, v_4 \in [0,1]} \mathcal{H}(x^*(t), v_1^*, v_2^*(t)); \tag{19}$$

with

$$\vartheta(t_f) = 0, \tag{20}$$

The principles outlined in Equation (19) are utilized to determine the adjoint system (adjoint variables) and optimal control variables. Based on these principles, the following result can be obtained.

Theorem 6. Suppose $\mathcal{S}_*, \mathcal{E}_*, \mathcal{I}_*, \mathcal{A}_*, \mathcal{H}_*$, and \mathcal{R}_* represent the optimal state solutions for the system, obtained using the combined optimal control variables (v_1^*, v_2^*) that were derived through the numerical solution of the optimality system. The optimal control problem is defined by the objective function (12) and the control system (13). Then \exists adjoint variables $\vartheta_1(t), \vartheta_2(t), \vartheta_3(t)$, and $\vartheta_4(t), \vartheta_5(t), \vartheta_6(t)$ satisfy

$$\begin{aligned}
 \vartheta_1'(t) &= -\mathcal{A}_1 + (\vartheta_2 - \vartheta_1) \varphi \mathcal{I}_* + (\vartheta_2 - \vartheta_1) \varphi q \mathcal{H}_* - \eta_0 \vartheta_1, \\
 \vartheta_2'(t) &= -\mathcal{A}_2 + (\vartheta_4 - \vartheta_2) \varphi N^* + (\chi + \eta_0) \vartheta_2 - \vartheta_1 v_1^* - \vartheta_3 \zeta, \\
 \vartheta_3'(t) &= -\mathcal{A}_3 + (\vartheta_2 - \vartheta_1) \varphi \mathcal{S}_* + (\vartheta_5 - \vartheta_3) \vartheta_a + (\vartheta_6 - \vartheta_3) \vartheta_1 + (\vartheta_6 - \vartheta_3) v_1(t) - v_1 \vartheta_3, \\
 \vartheta_4'(t) &= -\mathcal{A}_4 + (v_2 - u_0) \vartheta_4, \\
 \vartheta_5'(t) &= -\mathcal{A}_5 - (\vartheta_2 - \vartheta_1) \varphi q \mathcal{S}_* + (\vartheta_6 - \vartheta_5) \vartheta_\vartheta - (u_0 + v_2) \vartheta_5, \\
 \vartheta_6'(t) &= -\mathcal{A}_6 + u_0 \vartheta_6,
 \end{aligned}
 \tag{21}$$

with boundary conditions.

Additionally, the optimal control parameters $v_1(t)$ and $v_2(t)$ are obtained through numerical solutions of the optimality problem and are presented below.

$$v_1^*(t) = \max\{\min\{\frac{(\vartheta_6 - \vartheta_3) \mathcal{I}_*}{B_1}, 1\}, 0\}, \tag{22}$$

$$v_2^*(t) = \max\{\min\{\frac{(\vartheta_6 - \vartheta_5) \mathcal{H}_*}{B_2}, 1\}, 0\}. \tag{23}$$

Proof. The adjoint problem described by Equation (21) is obtained through the uses of the Pontryagin Maximum Principle given by Equation (19), while the transversal conditions

arise from $\vartheta(T) = 0$. The set of optimal functions v_1^*, v_2' is obtained using $\frac{\partial H}{\partial u}$. In the following section, we present numerical solutions to the optimality system in order to provide a clearer understanding for the reader, as opposed to relying solely on analytical results. The optimality problem is expressed by several components, including the control problem (13), the adjoint model (21), the boundary (terminal) conditions, and the optimal control functions. By solving these components numerically, we can gain valuable insights into the behavior of the system and assess its performance. □

6.2. Results and Discussion for Optimal Control

We utilize the Runge–Kutta method of order four to solve the optimal control system (13), in order to investigate the effects of self-care and treatment. To find the solution of the state system (12) with initial conditions in the time interval $[0, 50]$, we employ the forward Runge–Kutta procedure. Similarly, the backward Runge–Kutta technique is used to solve the adjoint system (21) in the same interval with the assistance of the transversality condition. Below are the parameters that we used for the simulation: $bN = 0.0071$; $\varphi = 0.00041$; $q = 0.0000123$; $\chi = 0.0000123$; $\zeta = 0.0000123$; $\vartheta_1 = 0.003907997$; $\vartheta_a = 0.98$; $\vartheta_\vartheta = 0.0000404720925$; $q = 0.017816$; $\rho = 0.00007$; and $\eta_0 = 0.00997$. The weight constants c_1, c_2, c_3 , and c_4 were chosen based on biological feasibility. Specifically, we set $c_1 = 0.6610000$, $c_2 = 0.54450$, $c_3 = 0.0090030$, $c_4 = 0.44440$. The results obtained from the simulations are presented in Figures 4 and 5.

Figures 4 and 5 show the variations in the number of all compartments with and without control measures implemented.

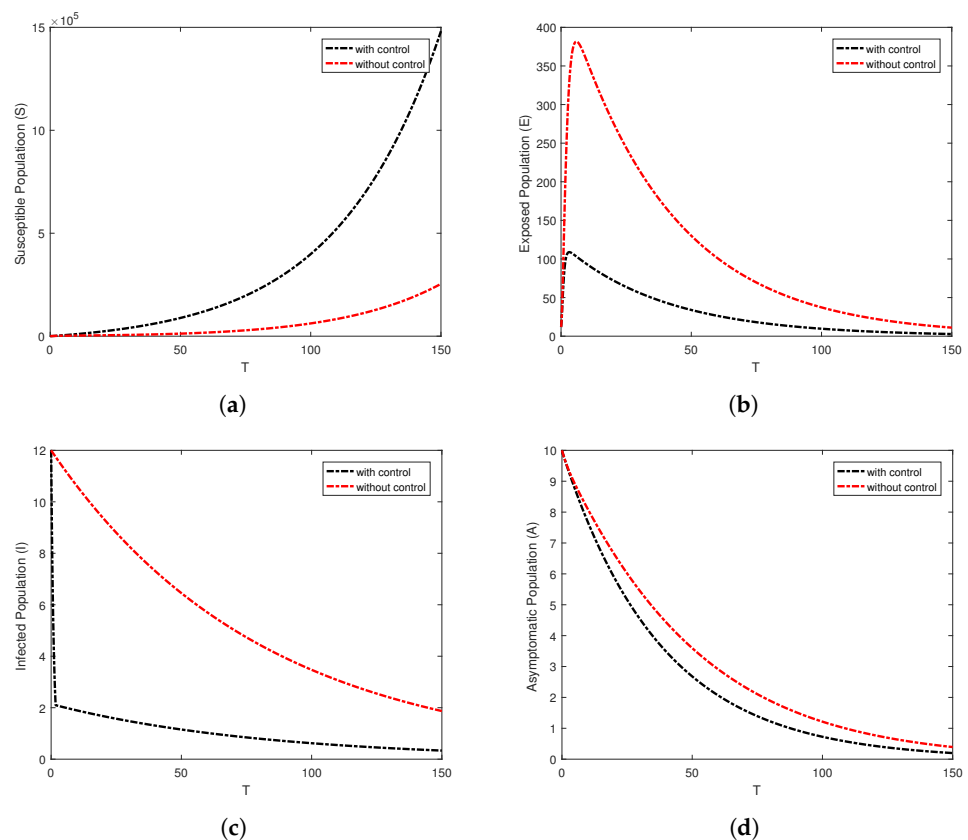


Figure 4. The visual representations demonstrate the changes in the compartmental population over time, comparing the scenarios with and without control measures implemented. (a) Susceptible populace; (b) exposed populace; (c) infected population; (d) asymptomatic population.

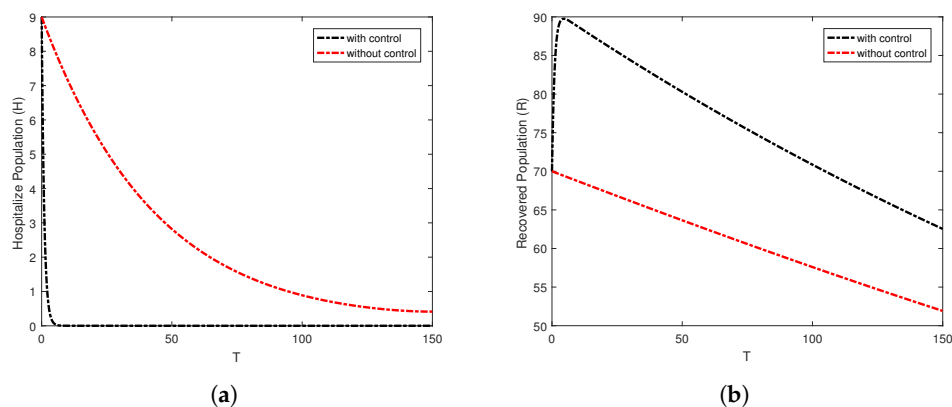


Figure 5. The visual representations demonstrate the changes in the compartmental population over time, comparing the scenarios with and without control measures implemented. (a) Hospitalized population; (b) recovered population.

7. Conclusions

The objective of this study is to develop a more realistic mathematical model that captures the transmission dynamics of the MERS-CoV. This is accomplished by introducing new parameters for the birth and death rates in the host populace. The threshold number R_0 is a measure used to estimate the potential spread of a disease within a populace, and it can be calculated from a model to quantify the transmissibility of MERS-CoV. The model is analyzed using stability theory to identify conditions for local and global stability, and the most sensitive parameter is determined through a sensitivity analysis of R_0 . An optimal control problem is formulated with the goal of minimizing the number of infected persons and maximizing the number of recoveries in the population. The effectiveness of the approach is verified through numerical simulations, which demonstrate the stability of the results.

Author Contributions: Conceptualization, B.F., M.Y. and M.u.R.; methodology, A.A. and S.A.; software, B.F.; validation, M.Y. and M.u.R.; formal analysis, M.Y.; investigation, A.A.; resources, S.A.; data curation, B.F.; writing—original draft preparation, B.F., M.Y. and M.u.R.; writing—review and editing, M.Y. and A.A.; supervision, S.A. All authors have read and agreed to the published version of the manuscript.

Funding: This research received no external funding.

Data Availability Statement: Not applicable.

Acknowledgments: The researchers would like to acknowledge Deanship of Scientific Research, Taif University for funding this work.

Conflicts of Interest: The authors declare no conflict of interest.

References

1. AlTawfiq, J.A.; Hinedi, K.; Ghandour, J. Middle East respiratory syndrome coronavirus: A case-control study of hospitalized patients. *Clin. Infect. Dis.* **2014**, *59*, 160–165. [[CrossRef](#)] [[PubMed](#)]
2. Azhar, E.I.; Kafrawy, E.I.; Hassan, S.A.; Al-Saeed, A.M.; Hashem, M.S.; Madani, A.M. Evidence for camel to human transmission of MERS coronavirus. *N. Engl. J. Med.* **2014**, *370*, 2499–2505. [[CrossRef](#)] [[PubMed](#)]
3. Arabi, Y.M.; Arifi, A.A.; Balkhy, H.H. Clinical course and outcomes of critically ill patients with Middle East respiratory syndrome coronavirus infection. *Ann. Intern. Med.* **2014**, *160*, 389–397. [[CrossRef](#)] [[PubMed](#)]
4. Madani, T.A.; Azhar, E.I.; Hashem, A.M. Evidence for camel-to-human transmission of MERS coronavirus. *N. Engl. J. Med.* **2014**, *371*, 1360. [[PubMed](#)]
5. Breban, R.; Riou, J.; Fontanet, A. Interhuman transmissibility of Middle East respiratory coronavirus: Estimation of pandemic risk. *Lancet* **2013**, *382*, 694–699. [[CrossRef](#)]
6. Fisman, D.N.; Ashleigh, R.T. The epidemiology of MERS-CoV. *Lancet Infect. Dis.* **2014**, *14*, 6–7. [[CrossRef](#)]

7. Zhong, N.S.; Zheng, B.J.; Li, Y.M.; Poon, L.L.M.; Xie, Z.H.; Chan, K.H.; Li, P.H.; Tan, S.Y.; Chang, Q.; Xie, J.P.; et al. Epidemiology and cause of severe acute respiratory syndrome (SARS) in Guangdong, People's Republic of China, in February, 2003. *Lancet* **2003**, *362*, 1353–1358. [[CrossRef](#)]
8. Ksiazek, T.G.; Erdman, D.; Goldsmith, C.S.; Zaki, S.R.; Peret, T.; Emery, S.; Tong, S.; Urbani, C.; Comer, J.A.; Lim, W.; et al. A novel coronavirus associated with severe acute respiratory syndrome. *N. Engl. J. Med.* **2003**, *348*, 1953–1966. [[CrossRef](#)]
9. Zaki, A.M.; Van Boheemen, S.; Bestebroer, T.M.; Osterhaus, A.D.; Fouchier, R.A. Isolation of a novel coronavirus from a man with pneumonia in Saudi Arabia. *N. Engl. J. Med.* **2012**, *367*, 1814–1820. [[CrossRef](#)]
10. Ciotti, M.; Ciccozzi, M.; Terrinoni, A.; Jiang, W.C.; Wang, C.B.; Bernardini, S. The COVID-19 pandemic. *Crit. Rev. Clin. Lab. Sci.* **2020**, *57*, 365–388. [[CrossRef](#)]
11. Mandal, M.; Jana, S.; Nandi, S.K.; Khatua, A.; Adak, S.; Kar, T.K. A model based study on the dynamics of COVID-19: Prediction and control. *Chaos Solitons Fractals* **2020**, *136*, 109889. [[CrossRef](#)] [[PubMed](#)]
12. Atede, A.O.; Omame, A.; Inyama, S.C. A fractional order vaccination model for COVID-19 incorporating environmental transmission: A case study using Nigerian data. *Bull. Biomath.* **2023**, *1*, 78–110. [[CrossRef](#)]
13. Shen, Z.H.; Chu, Y.M.; Khan, M.A.; Muhammad, S.; Al-Hartomy, O.A.; Higazy, M. Mathematical modeling and optimal control of the COVID-19 dynamics. *Results Phys.* **2021**, *31*, 105028. [[CrossRef](#)] [[PubMed](#)]
14. Alqarni, M.S.; Alghamdi, M.; Muhammad, T.; Alshomrani, A.S.; Khan, M.A. Mathematical modeling for novel coronavirus (COVID-19) and control. *Numer. Methods Partial. Differ. Equ.* **2022**, *38*, 760–776. [[CrossRef](#)]
15. Tsay, C.; Lejarza, F.; Stadtherr, M.A.; Baldea, M. Modeling, state estimation, and optimal control for the US COVID-19 outbreak. *Sci. Rep.* **2020**, *10*, 10711. [[CrossRef](#)]
16. Libotte, G.B.; Lobato, F.S.; Platt, G.M.; Neto, A.J.S. Determination of an optimal control strategy for vaccine administration in COVID-19 pandemic treatment. *Comput. Methods Programs Biomed.* **2020**, *196*, 105664. [[CrossRef](#)]
17. Ullah, I.; Ahmad, S.; Al-Mdallal, Q.; Khan, Z.A.; Khan, H.; Khan, A. Stability analysis of a dynamical model of tuberculosis with incomplete treatment. *Adv. Differ. Equ.* **2020**, *2020*, 499. [[CrossRef](#)]
18. Hajji Mohamed, A.; Al-Mdallal, Q. Numerical simulations of a delay model for immune system-tumor interaction. *Sultan Qaboos Univ. J. Sci. (SQUJS)* **2018**, *23*, 19–31.
19. Asif, M.; Haider, N.; Al-Mdallal, Q.; Khan, I. A Haar wavelet collocation approach for solving one and two-dimensional second-order linear and nonlinear hyperbolic telegraph equations. *Numer. Methods Partial. Differ. Equ.* **2020**, *36*, 1962–1981. [[CrossRef](#)]
20. Kermack, W.O.; McKendrick, A.G. Contributions to the mathematical theory of epidemics, part 1. *Proc. R. Soc. Edinburgh. Sect. A Math.* **1927**, *115*, 700–721.
21. Cauchemez, S.; Fraser, C.; Van Kerkhove, M.D.; Donnelly, C.A.; Riley, S.; Rambaut, A.; Enouf, V.; van der Werf, S.; Ferguson, N.M. Middle East respiratory syndrome coronavirus: Quantification of the extent of the epidemic, surveillance biases, and transmissibility. *Lancet Infect. Dis.* **2013**, *14*, 50–56. [[CrossRef](#)]
22. Chowell, G.; Blumberg, S.; Simonsen, L.; Miller, M.A.; Viboud, C. Synthesizing data and models for the spread of MERS-CoV, 2013: Key role of index cases and hospital transmission. *Epidemics* **2014**, *9*, 40–51. [[CrossRef](#)] [[PubMed](#)]
23. Assiri, A.; Al-Tawfiq, J.A.; Al-Rabeeah, A.A.; Al-Rabiah, F.A.; Al-Hajjar, S.; Al-Barrak, A. Epidemiological, demographic, and clinical characteristics of 47 cases of Middle East respiratory syndrome coronavirus disease from Saudi Arabia: A descriptive study. *Lancet Infect. Dis.* **2013**, *13*, 752–761. [[CrossRef](#)] [[PubMed](#)]
24. Li, B.; Eskandari, Z.; Avazzadeh, Z. Dynamical behaviors of an SIR epidemic model with discrete time. *Fractal Fract.* **2022**, *6*, 659. [[CrossRef](#)]
25. Li, B.; Eskandari, Z. Dynamical analysis of a discrete-time SIR epidemic model. *J. Frankl. Inst.* **2023**, *360*, 7989–8007. [[CrossRef](#)]
26. Li, B.; Eskandari, Z.; Avazzadeh, Z. Strong resonance bifurcations for a discrete-time prey–predator model. *J. Appl. Math. Comput.* **2023**, *69*, 2421–2438. [[CrossRef](#)]
27. Jiang, X.; Li, J.; Li, B.; Yin, W.; Sun, L.; Chen, X. Bifurcation, chaos, and circuit realisation of a new four-dimensional memristor system. *Int. J. Nonlinear Sci. Numer. Simul.* **2022**. [[CrossRef](#)]
28. Sabbar, Y. Asymptotic extinction and persistence of a perturbed epidemic model with different intervention measures and standard lévy jumps. *Bull. Biomath.* **2023**, *1*, 58–77. [[CrossRef](#)]
29. Adoum, A.H.; Hagggar, M.S.D.; Ntaganda, J.M. Mathematical modelling of a glucose-insulin system for type 2 diabetic patients in Chad. *Math. Model. Numer. Simul. Appl.* **2022**, *2*, 244–251. [[CrossRef](#)]
30. Ahmed, I.; Akgül, A.; Jarad, F.; Kumam, P.; Nonlaopon, K. A Caputo-Fabrizio fractional-order cholera model and its sensitivity analysis. *Math. Model. Numer. Simul. Appl.* **2023**, *3*, 170–187. [[CrossRef](#)]
31. Singh, T.; Vaishali; Adlakha, N. Numerical investigations and simulation of calcium distribution in the alpha-cell. *Bull. Biomath.* **2023**, *1*, 40–57. [[CrossRef](#)]
32. Odionyenma, U.B.; Ikenna, N.; Bolaji, B. Analysis of a model to control the co-dynamics of Chlamydia and Gonorrhoea using Caputo fractional derivative. *Math. Model. Numer. Simul. Appl.* **2023**, *3*, 111–140. [[CrossRef](#)]
33. Yao, T.-T.; Qian, J.-D.; Zhu, W.-Y.; Wang, Y.; Wang, G.-Q. A systematic review of lopinavir therapy for SARS coronavirus and MERS coronavirus—A possible reference for coronavirus disease-19 treatment option. *J. Med. Virol.* **2020**, *92*, 556–563. [[CrossRef](#)] [[PubMed](#)]

34. Fatima, B.; Yavuz, M.; Rahman, M.u.; Al-Duais, F.S. Modeling the epidemic trend of middle eastern respiratory syndrome coronavirus with optimal control. *Math. Biosci. Eng.* **2023**, *20*, 11847–11874. [[CrossRef](#)]
35. Afshar, Z.M.; Ebrahimpour, S.; Javanian, M.; Koppolu, V.; Vasigala, V.K.R.; Hasanpour, A.H.; Babazadeh, A. Coronavirus disease 2019 (COVID-19), MERS and SARS: Similarity and difference. *J. Acute Dis.* **2020**, *9*, 194–199.
36. Ahmad, S.; Dong, Q.; Rahman, M.u. Dynamics of a fractional-order COVID-19 model under the nonsingular kernel of Caputo-Fabrizio operator. *Math. Model. Numer. Simul. Appl.* **2022**, *2*, 228–243. [[CrossRef](#)]
37. ur Rahman, M.; Arfan, M.; Baleanu, D. Piecewise fractional analysis of the migration effect in plant-pathogen-herbivore interactions. *Bull. Biomath.* **2023**, *1*, 1–23. [[CrossRef](#)]
38. Yunhwan, K.; Sunmi, L.; Chaeshin, C.; Seoyun, C.; Saeme, H.; Youngseo, S. The Characteristics of Middle Eastern Respiratory Syndrome Coronavirus Transmission Dynamics in South Korea. *Osong Public Health Res. Perspect.* **2016**, *7*, 49–55.
39. Driessch, V.; Watmough, J. Reproduction numbers and sub threshold endemic equilibria for compartmental models of disease transmission. *Math. Biosci.* **2002**, *180*, 29–48. [[CrossRef](#)]
40. Van Den Driessche, P.; Watmough, J. *Mathematical Epidemiology*; Springer: Berlin/Heidelberg, Germany, 2008.
41. Chitnis, N.; Cushing, J.M.; Hyman, J.M. Bifurcation analysis of a mathematical model for malaria transmission. *SIAM J. Appl. Math.* **2006**, *67*, 24–45. [[CrossRef](#)]
42. Khan, T.; Zaman, G.; Chohan, M.I. The transmission dynamic and optimal control of acute and chronic hepatitis B. *J. Biol. Dyn.* **2017**, *11*, 172–189. [[CrossRef](#)]
43. Zaman, G.; Han Kang, Y.; Jung, I.H. Stability analysis and optimal vaccination of an SIR epidemic model. *Biosystems* **2008**, *93*, 240–249. [[CrossRef](#)] [[PubMed](#)]
44. LaSalle, J.P. *The Stability of Dynamical System*; SIAM: Philadelphia, PA, USA, 1976.
45. LaSalle, J.P. Stability of nonautonomous system. *Nonlinear Anal.* **1976**, *1*, 83–90. [[CrossRef](#)]
46. Khan, T.; Ullah, Z.; Ali, N.; Zaman, G. Modeling and control of the hepatitis b virus spreading using an epidemic model. *Chaos Solitons Fractals* **2019**, *124*, 1–9. [[CrossRef](#)]
47. Kamien, M.; Schwartz, N. *Dynamic Optimization*, 2nd ed.; North-Holland: Amsterdam, The Netherlands, 1991.
48. Hattaf, K.; Yousfi, N. Optimal control of a delayed HIV infection model with immune response using an efficient numerical method. *Int. Sch. Res. Not.* **2012**, *2012*, 215124. [[CrossRef](#)]
49. Evirgen F.; Ozköse, F.; Yavuz, M.; Ozdemir, N. Real data-based optimal control strategies for assessing the impact of the Omicron variant on heart attacks. *AIMS Bioeng.* **2023**, *10*, 218–239. [[CrossRef](#)]
50. Lashari, A.A.; Zaman, G. Global dynamics of vector-borne diseases with horizontal transmission in host population. *Comput. Math. Appl.* **2001**, *61*, 745–754. [[CrossRef](#)]
51. Aseev, S.M.; Kryazhinskii, A.V. The Pontryagin maximum principle and optimal economic growth problems. *Proc. Steklov Inst. Math.* **2007**, *257*, 1–255. [[CrossRef](#)]

Disclaimer/Publisher’s Note: The statements, opinions and data contained in all publications are solely those of the individual author(s) and contributor(s) and not of MDPI and/or the editor(s). MDPI and/or the editor(s) disclaim responsibility for any injury to people or property resulting from any ideas, methods, instructions or products referred to in the content.